Chinese Chemical Letters 35 (2024) 109251

Contents lists available at ScienceDirect

Chinese Chemical Letters

journal homepage: www.elsevier.com/locate/cclet

Molecular engineering towards dual surface local polarization sites on poly(heptazine imide) framework for boosting H_2O_2 photo-production

Zhenchun Yang[a], Bixiao Guo[b], Zhenyu Hu[a], Kun Wang[a], Jiahao Cui[a], Lina Li[a], Chun Hu[a], Yubao Zhao[a,*]

[a] Key Laboratory for Water Quality and Conservation of the Pearl River Delta, Ministry of Education, Institute of Environmental Research at Greater Bay, Guangzhou University, Guangzhou 510006, China
[b] Department of Environmental Science and Engineering, Guangzhou University, Guangzhou 510006, China

ARTICLE INFO

Article history:
Received 7 July 2023
Revised 7 October 2023
Accepted 26 October 2023
Available online 2 November 2023

Keywords:
Photocatalysis
Hydrogen peroxide production
Carbon nitride framework
Surface functionalization
ORR

ABSTRACT

The selective 2e⁻ ORR reaction on polymeric carbon nitride framework is one of the most promising approaches for solar-driven hydrogen peroxide production. Poly(heptazine imide) (PHI) as a class of K^+-incorporated crystalline carbon nitride framework, is highly active for photocatalytic H_2O_2 production. An upgrade on the H_2O_2 photoproduction performance of PHI is realized and the mechanistic insights are revealed in this work. By photochemical reaction, the electron withdrawing groups of hydroxyl group and cyano group are grafted on the surface of PHI frameworks. The dual polarization sites on the surface contribute significantly to the enhancement of the exciton dissociation. The optimized PHI with dual polarization sites exhibits a remarkable photocatalytic H_2O_2 production performance, which is 2 times of the active pristine PHI. Most importantly, the photochemical reaction method is generally applicable to improve the exciton dissociation of a wide range of polymeric carbon nitride frameworks with various structure and compositions; and the thiourea-derived polymeric carbon nitride framework with dual surface polarization sites exhibits a remarkable photocatalytic performance with a high H_2O_2 production rate of 40.5 mmol h^{-1} g^{-1}.

Hydrogen peroxide (H_2O_2) is a versatile chemical, which finds wide applications in a plethora of fields, such as energy conversion, environmental remediation, chemical industry medical treatment [1–3]. The anthraquinone-based method is the traditionally applied in H_2O_2 production. However, it requires fossil-fuel derived H_2 as the feed stock, and the operation process is complicated and energy intensive [4,5]. A sustainable way for the production of such a useful chemical is highly desired. Photocatalysis, using the clean and inexhaustible solar light as the energy source, has demonstrated its appealing sustainability in water splitting, CO_2 reduction, pollutants degradation, and organics conversions, *etc.* [6–11]. Production of H_2O_2 *via* photocatalytic dioxygen reduction owns the overwhelming advantages of remarkable eco-friendliness and cost-effectiveness, and thus attracts intensive research interest [12,13]. Carbon-based active sites are especially favorable for selective 2e⁻ oxygen reduction reaction (2e⁻ ORR) [14–18], and diverse organic and/or hybrid photocatalysts are capable of driving the selective 2e⁻ oxygen reduction reaction (2e⁻ ORR), such as covalent organic framework (COF), polymeric carbon nitride framework (PCN), phenol-formaldehyde resin and metal-organic frameworks (MOFs) [19–24]. PCN framework in particular, with a unique modular structure, could be precisely designed in molecular level and synthesized with ease through thermal polymerization process. Moreover, PCN also possesses additional favorable features of non-toxicity, physiochemical stability, and low-cost synthesis, *etc.* [25–27]. PCN photocatalyzed 2e⁻ ORR is therefore one of the most promising approaches for sustainable H_2O_2 production. However, low exciton dissociation is the major barrier impeding the improvement of the solar-to-chemical conversion efficiency [28–30]. Various efforts has been devoted to enhancing the exciton dissociation in organic frameworks *via* nanoarchitectonics, in which the construction of local polarizations is revealed to be intrinsically favorable for exciton dissociation [31–37].

As a fascinating class in the PCN family, poly(heptazine imide) (PHI) frameworks own metal cations induced local polarization centers, which exhibit remarkable photocatalytic performance [38–40]; and the efforts on the nano-structure manipulation further boost the efficiency of photocatalytic H_2O_2 production [41,42]. In

* Corresponding author.
E-mail address: ybzhao@gzhu.edu.cn (Y. Zhao).

https://doi.org/10.1016/j.cclet.2023.109251
1001-8417/

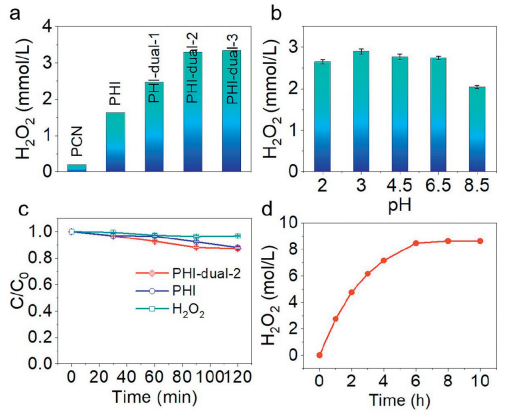

Fig. 1. Photocatalytic performance of the samples for hydrogen peroxide production. (a) Comparison of the photocatalytic performance of a series of PHI frameworks. (b) The impact of pH on the photocatalytic hydrogen peroxide production. (c) The photocatalytic decomposition of 10.0 mmol/L H_2O_2 on photocatalysts. (d) Long-term running performance of PHI-dual-2 in photocatalytic H_2O_2 production.

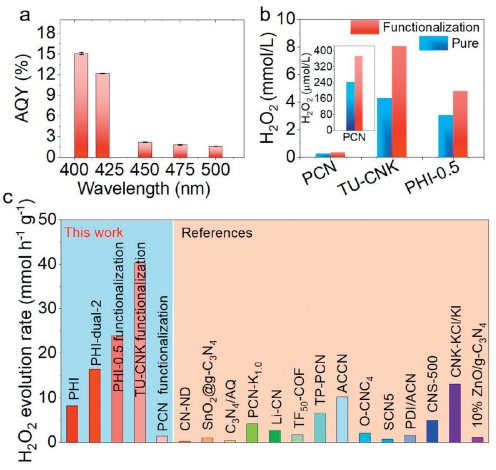

Fig. 2. (a) Apparent quantum yield of PHI-dual-2 in the photocatalytic H_2O_2 production reaction. (b) Enhancement of the photocatalytic H_2O_2 production by surface functionalization on other photocatalysts. (c) Comparing of the work and reference catalysts for H_2O_2 evolution rate (experimental details in Table S1 in Supporting information).

spite of the advances in this area, the knowledge on the structure-activity relationship is relatively in lack. Novel approaches towards specified nanoarchitectures favorable for exciton dissociation is highly desired. Herein, we developed a facile method based on the photochemical reaction for grafting the dual polar moieties of hydroxyl and cyano groups on the surface of the PHI framework. The dual polarization sites on the surface remarkably extend the life time of the charge carriers and improve the charge transfer process. The molecularly engineered PHI exhibits a remarkable photocatalytic H_2O_2 production rate, which is 16.1 and 2.0 times of that on PCN and pristine PHI, respectively. Additionally, the molecular engineering could be applicable to the construction of dual polarization sites on the surface of various PCN frameworks and some covalent organic frameworks, and thereby improve their catalytic performance in photocatalytic $2e^-$ ORR.

As shown in Scheme S1 (Supporting information), PHI was synthesized *via* polymerization of 5-aminotetrazole (5-AT) in a eutectic salt mixture of LiCl/KCl at 550 °C. The following molecular engineering on the surface of PHI framework was realized by the photochemical reaction in aqueous suspension containing PHI, KSCN, and $Na_2S_2O_8$. The optimum photochemical reaction time was 30 min (Fig. S1 in Supporting information). The functionalized PHI frameworks with dual surface polarization sites are denoted by PHI-dual-X, wherein X equals to 1, 2, and 3, respectively for the samples synthesized with KSCN and $K_2S_2O_8$ loading of 0.5 g/1.0 g, 1.0 g/1.0 g, 1.5 g/1.0 g in the suspension for photochemical reaction.

The photocatalytic H_2O_2 production performance was measured under the irradiation of a solar simulator with light intensity of 100 mW/cm^2 in the presence of 5 vol% ethanol. As shown in Fig. 1a, 1 h irradiation on PHI produces 1.63 mmol/L H_2O_2, while PHI-dual-1 and PHI-dual-2 catalyzed reaction systems, respectively, generate 2.47 mmol/L and 3.29 mmol/L in 1 h. Further adjusting the photochemical reaction conditions is unable to improve the performance of the catalysts any more, and PHI-dual-3 exhibits a catalytic performance close to that of PHI-dual-2. The H_2O_2 production rate of PHI-dual-2 could reach a high value of 16.5 μmol h^{-1} mg^{-1}, which is 2.0 and 16.1 times of that on the pristine PHI and PCN, respectively.

Protonation reaction is one of the critical steps in $2e^-$ ORR, and the impact of the acidity of the solution was thus examined. As shown in Fig. 1b, the photocatalytic performance of PHI-dual-2 increases gradually with acidity of the suspension, while the basic solution obviously impedes the photo-production of H_2O_2. The photocatalytic H_2O_2 decomposition is critical for the accumulation of H_2O_2 in the reaction system; as shown in Fig. 1c, the concentration of H_2O_2 keeps stable in 2 h irradiation without photocatalysts. PHI and PHI-dual-2 all show negligible catalytic activity for H_2O_2 decomposition, which is favorable for the accumulation of the H_2O_2 in reaction process. Fig. 1d shows the long-term stability of PHI-dual-2, and the H_2O_2 concentration reaches a high value of 8.47 mmol/L at the reaction time of 6 h. There are no obvious distinctions in nano-structure and surface functional groups of PHI-dual-2 before and after 10 h of reaction (Figs. S2 and S3 in Supporting information), indicating the structural stability of the framework.

To evaluate the efficiency of the solar-driven H_2O_2 production, apparent quantum yield (AQY) was examined. As shown in Fig. 2a, PHI-dual-2 exhibits a remarkable AQY of 15.1% at 405 nm, and 12.2% at 420 nm. For simulating the continuous H_2O_2 photo-production, we then measured the photo-production of H_2O_2 in flow mode employing a continuous serial micro-batch flow photoreactor with white LED arrays as the light source ($\lambda \geq 400$ nm) (Fig. S4 in Supporting information). The H_2O_2 concentration could reach 2.48 mmol/L at a retention time of 48 min with PHI-dual-2 loading of 1 g/L. When the catalytic loading increases to 3 g/L, the amount of H_2O_2 raises to 4.0 mmol/L in 48 min photocatalytic reaction.

To explore the general applicability of this strategy for boosting the catalytic performance of the polymeric carbon nitride family for $2e^-$ ORR process, a series of polymeric carbon nitride frameworks with distinct compositions and physiochemical properties were subjected to the photochemical reaction for grafting the surface polarization sites. As shown in Fig. 2b, a uniform enhancement of the photocatalytic performance of the pristine PCN, K^+-doped crystalline lamellar carbon nitride synthesized with thiol-urea (TU-CNK) on KCl crystal, and the engineered poly(heptazine imide) (PHI-0.5) is observed [41–43]. Particularly, the surface functionalization improves the performance of these photocatalysts by a factor of 1.5–1.9 in terms of the H_2O_2 production rate. Moreover, the H_2O_2 generation rates of the carbon nitride frameworks of this work are outstanding among the recently reported highly efficient photocatalytic reaction systems (Fig. 2c and Table S1 in Supporting information). It is especially worth noting that the H_2O_2 evolution rates of TU-CNK-modification could reach a remarkable high value of 40.3 mmol h^{-1} g^{-1}.

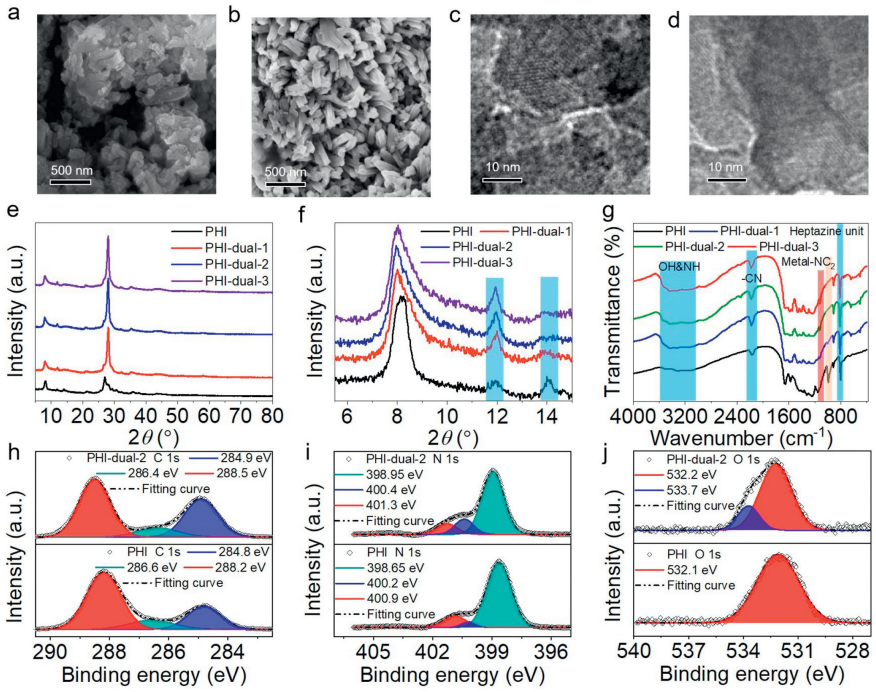

Fig. 3. Scanning electron microscopy (SEM) images of PHI (a) and PHI-dual-2 (b). Transmission electron microscopy (TEM) images of PHI (c) and PHI-dual-2 (d). (e, f) X-ray diffraction (XRD) patterns and (g) FTIR spectra of PHI, PHI-dual-1, PHI-dual-2 and PHI-dual-3. X-ray photoelectron spectra (XPS) of PHI and PHI-dual-2. (h) C 1s, (i) N 1s and (j) O 1s.

For understanding the rationale behind the superior photocatalytic performance of PHI with dual surface polarization sites, we then screened the structural features, photochemical properties, and photophysical behaviors of the photocatalysts. The morphology of PHI and PHI-dual-2 was visualized by microscopic techniques. As shown in Figs. 3a and b, both PHI and PHI-dual-2 show the morphology of array of columns. Figs. 3c and d are the transmission electron microscopy (TEM) images of PHI and PHI-dual-2, the layer stacking structure is clearly observed. The surface functionalization process could also lead to the exfoliation of the layer-stacking structure, and the BET surface area of PHI and PHI-dual-2 are 20.8 and 30.3 m^2/g, respectively (Fig. S5 in Supporting information).

In X-ray diffraction (XRD) patterns, PHI shows diffraction peaks at 8.2° and 27.0°, which are assigned to (100) diffraction (ordered heptazine units) and (002) diffraction (layer stacking structure), respectively (Fig. 3e). PHI-dual-2 shows (100) and (002) diffraction peaks at 8.0° and 28.0°, respectively. The shift of (002) diffraction peaks of PHI-dual-2 as compared to PHI reveals that the inter-layer spacing of PHI-dual-2 is reduced by 0.012 nm. Reduced inter-layer spacing might be beneficial for enhancing exciton dissociation, due to the unique electronic transportation behavior of PCN frameworks; in particular, the free polarons diffuse in Brownian motion and are confined within the channel along the *c*-direction perpendicular to the plane of tri-*s*-triazine [44]. Moreover, the diffraction peaks at 11.9° and 14.0°, which are indexed to (110) and (010) diffractions, respectively (Fig. 3f). As compared to PHI, the (110) diffraction peak is strengthened and the (010) diffraction peak is weakened in the XRD profile of PHI-dual-2. These differences are speaking for the partial rearrangement of the layer-stacking structure in the surface functionalization process [45].

The differences in structure in molecular level were further examined with Fourier transform infrared (FTIR) spectroscopy. As shown in Fig. 3g, the absorption peaks at 803, 992 and 2183 cm^{-1} are assigned to the out-of-plane bending vibration of the heptazine unit, the C−N−C bond in the K^+-NC_2 moiety, and asymmetric vibration of the triple bond in the cyano group (−C≡N), respectively [46,47]. In the spectra of PHI-dual-X, the absorption peaks of the heptazine unit shift to 811 cm^{-1}, which indicates that surface functionalization decreases the electron density of the conjugated system (Fig. S6 in Supporting information). In addition, the intensity of the vibration peak resulting from K^+-NC_2 moiety is reduced, which is due to the decrease of K^+ in the framework during the photochemical reaction process. By inductively coupled plasma optical emission spectrometry (ICP-OES), the contents of K^+ in PHI and PHI-dual-2 are 8.6 wt% and 1.2 wt%, respectively. As compared with PHI, the vibration peaks at 2183 cm^{-1} are enhanced for PHI-dual-X, indicating increased amount of cyano group (−C≡N) in the framework.

Moreover, surface functionalization introduces a new peak at 1120 cm^{-1}, and this peak increases gradually from PHI-dual-1 to PHI-dual-3, demonstrating the presence of C−O group on PHI-dual-X [48,49]. Meanwhile, the broad peak at 2800–3400 cm^{-1}, which is attributed to N−H/O−H stretching vibration, is observed in the spectra of surface functionalized samples [50]. Based on the spectroscopy signals of C−O and N−H/O−H groups, the hydroxyl groups is proposed to be introduced by the photochemical process and is connected to the heptazine unit *via* C−O bond. According to the above-mentioned data analysis, it is proposed that the photochemical surface functionalization generates dual polarization sites of cyano group and hydroxyl group on the PHI framework.

X-ray photoelectron spectroscopy (XPS) was employed for investigating the chemical environment of the elements in PHI and PHI-dual-2 frameworks. XPS survey scans confirm the presence of C, N, O, and K in all samples (Figs. S7 and S8 in Supporting information). As shown in Fig. 3h, the C 1s signal of PHI-dual-2 is deconvoluted into three components at 284.9, 286.4, and 288.5 eV, which are, respectively, assigned to adventitious carbon (C−C or C=C), the carbon atoms connected to $-NH_x$, −OH or cyano groups, and the carbon atom in N−C=N unit in the heptazine unit [51–53]. Comparing with PHI, the peak of N−C=N shifts 0.3 eV toward high binding energy for PHI-dual-2. The peak shift is also observed in

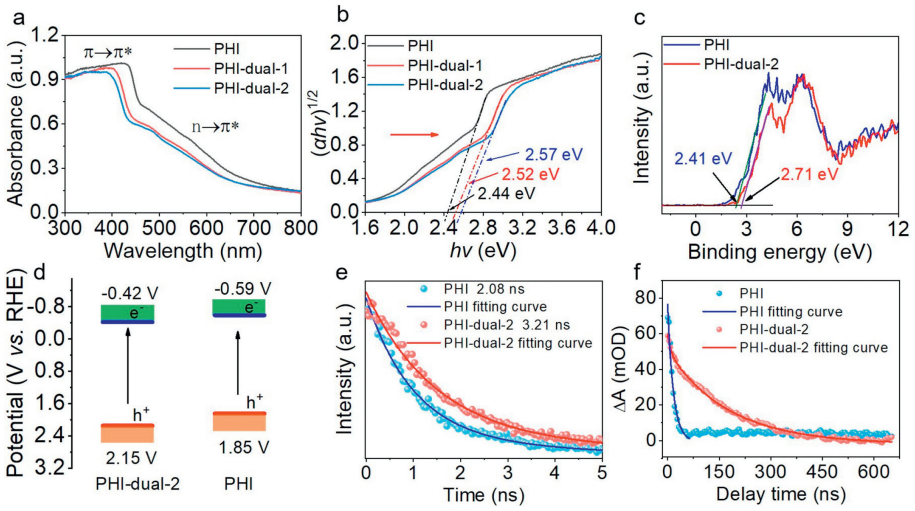

Fig. 4. (a) UV–vis diffuse reflectance spectra. (b) Curves of the transformed Kubelka-Munk function *versus* photon energy. (c) Valence band X-ray photoelectron spectra. (d) Band structure diagram. (e) Time-resolved photoluminescence (tr-PL) spectra of PHI and PHI-dual-2 under 300 nm excitation. (f) Femtosecond transient absorption spectroscopy (fs-TAS) decay kinetics profiles of the peak at the wavelength of 680 nm of PHI and PHI-dual-2 in aerobic conditions.

the N 1s signal. For PHI-dual-2, the XPS spectrum is deconvoluted into three peaks with the binding energies of 399.0 eV (pyridinic N), 400.4 eV (graphitic N), and 401.3 eV (bridging −NH−) (Fig. 3i) [54–57]. In contrast, deconvolution of the N 1s signal of PHI affords three peaks with binding energies of 398.7, 400.2, and 400.9 eV. XPS characterizations reveal that grafting of dual polarization sites reduces the electron density of the heptazine conjugation system.

By XPS, the C/N ratios on the surface of PHI-dual-2 and PHI are determined to be 1.01 and 1.36, respectively. However, elemental analysis demonstrates that PHI-dual-2 and PHI have the same C/N ratio. XPS and elemental analysis together reveal that the dual polarization sites are locating at the surface of the framework, rather than in the bulk. For a single particle under irradiation, the inhomogeneous chemical composition from the bulk to the surface could induce internal electric field, which is favorable for exciton dissociation. XPS profile of O 1s electron presents a single peak with binding energy of 532.2 eV, which is corresponded to the surface adsorbed H_2O and O_2 [51,58]; however, there is one new peak with binding energy of 533.7 eV observed in the O 1s signal of PHI-dual-2, revealing the presence of O−H in the framework (Fig. 3j) [51,59]. Additionally, the H content of PHI-dual-2 is obviously increased as compared with that of PHI (Table S3 in Supporting information). All these experimental analyses consistently support the formation of the hydroxyl group on the PHI framework during photochemical surface functionalization process.

Electron spin resonance (ESR) technique was employed for monitoring the single electron in the PHI framework. As shown in Fig. S9 (Supporting information), the singlet Lorenz line with a *g* value of 2.0035 is observed in the spectra of all the samples. This resonance signal originates from the unpaired electron of the sp^2 hybrid orbital of carbon atom in PHI framework [60]. Most importantly, the intensities of the singlet signal increase with the amount of the hydroxyl and cyano groups on the framework, revealing that the grafting of dual surface polarization sites alters the electronic structure of the conjugated polymeric systems.

For understanding the relationship between the molecular structure and the photocatalytic performance, the photo-physical and chemical properties of the catalyst were explored. As the excitation is the initial step of a photocatalytic process, we thus examine the photon absorption properties first. As shown in Fig. 4a, blue shifts of the absorption of PHI-dual-1 and PHI-dual-2 demonstrate an extended band gap, which is reasonable as the overall electron density of the conjugated systems are lowered by grafting of the surface polarization sites. In the Tauc plots from Kubelka-Munk function transformation, the optical band gaps of PHI, PHI-dual-1 and PHI-dual-2 are determined to be 2.44, 2.52 and 2.78 eV, respectively (Fig. 4b).

The valence band position is determined by XPS valence band spectra using Eq. 1:

$$E_{NHE} = \Phi + E_{VB-XPS} - 4.44 \quad (1)$$

wherein E_{NHE} is the potential *versus* normal hydrogen electrode, Φ is the electron work function of the analyzer (3.88 eV) [61,62].

The valence bands of PHI and PHI-dual-2 are 2.15 V (*vs.* RHE) and 1.85 V (*vs.* RHE), respectively (Figs. 4c and d). The conduction band potentials of PHI and PHI-dual-2 are thereby, respectively, determined to be −0.42 V (*vs.* RHE) and −0.59 V (*vs.* RHE) (Fig. 4d). The surface functionalization enhances the oxidation power of the PHI framework, which is beneficial for rapid hole oxidation reaction and charges separation. The enhanced charge separation was further confirmed by time-resolved photoluminescence (tr-PL) spectroscopy. As shown in Fig. 4e and Table S4 (Supporting information), PHI-dual-2 exhibits a slower decay kinetics than that of PHI, for example, 3.21 ns and 2.08 ns for PHI-dual-2 and PHI, respectively. The behavior of the polaron electrons was further investigated by monitoring the decay kinetics at 680 nm in the ns to μs time scale. As shown in Fig. 4f, the polaron electrons have a longer lifetime for PHI-dual-2 ($\tau_1 = 9.3 \pm 1.9$ ns, $\tau_2 = 177.0 \pm 3.4$ ns) than that of PHI ($\tau = 16.6 \pm 1.9$ ns). The prolonged lifetime of polaron electrons of PHI-dual-2 allows enhanced charge diffusion to the surface, which are favorable for surface electron transfer reaction towards dioxygen reduction. The charge transfer properties of the frameworks were further examined in a photoelectrochemical reaction system. As shown in Fig. S10a (Supporting information), the photo-current performances of the electrodes with PHI-dual-1 and PHI-dual-2 frameworks as the active materials are obviously stronger than that of the PHI framework. Moreover, in the Nyquist plots, PHI-dual-2 shows impedance lower than that of PHI, indicating the improved charge migration by the construction of the dual surface polarization sites (Fig. S10b in Supporting information).

We then focused on the H_2O_2 generation reaction initiated by the interfacial electron transfer from photocatalyst to the surface adsorbed dioxygen. A series of quenching reactions and spectroscopic analysis by electron spin resonance were thereby performed in the PHI-dual-2 photocatalyzed reaction system. As shown in Fig. S11a (Supporting information), H_2O_2 generation is sensitively im-

pacted by the atmosphere of the reaction suspension, for example, 1-h photocatalytic reaction generates 3.31 mmol/L and 1.85 mmol/L H_2O_2 in oxygen and air, respectively. There is 0.15 mmol/L H_2O_2 detected under N_2 atmosphere, which could result from the reduction of the residual dissolved oxygen in the suspension. One electron reduction of dioxygen could produce superoxide radical ($O_2^{\bullet-}$), and parabenzoquinone (PBQ) is usually employed for quenching $O_2^{\bullet-}$ [63,64]. H_2O_2 production is significantly attenuated by the presence of PBQ in the reaction system. Additionally, in the presence of L-histidine, an efficient scavenger for singlet oxygen ($^1O_2$), the H_2O_2 photo-production is also obviously impeded. These quenching experiments demonstrate that $O_2^{\bullet-}$ and $^1O_2$ could be the critical intermediates for H_2O_2 production.

By using ESR technique, the reactive oxygen species (ROS) in the reaction system were further explored. In Fig. S11b (Supporting information), with 5,5-dimethyl-1-pyrroline *N*-oxide (DMPO) as the spin trapping agent, the quartet signal could be translated into the generation of hydroxyl radical ($^{\bullet}OH$), which might result from the partial decomposition of H_2O_2. With DMPO as the spin trapping agent for superoxide radicals, the characteristic peaks of the trapped $O_2^{\bullet-}$ appear upon light irradiation (Fig. S11c in Supporting information), which demonstrates the generation of $O_2^{\bullet-}$ in the reaction system. Using 2,2,6,6-tetramethylpiperidine (TEMP) as the spin trapping agent for $^1O_2$, the characteristic triplet signal is observed in the system (Fig. S11d in Supporting information), revealing the production of $^1O_2$. Moreover, the intensities of the signals increase with reaction time. Together with the data analysis on the quenching experiments, the $^1O_2$ and $O_2^{\bullet-}$ are proposed to be the essential intermediates for the production of the H_2O_2 *via* proton/electron extraction from the proton/electron donor [15,65].

Poly(heptazine imide) as a fascinating class of crystalline carbon nitride framework, exhibits a remarkable photocatalytic H_2O_2 production performance. Using the photochemical reaction approach, the electron withdrawing groups of hydroxyl and cyano groups are grafted on the surface of PHI frameworks, leading to dual surface polarization sites. The presence of dual surface polarization sites significantly extends charge carrier lifetime and improves charge transmission performance of the polymeric framework. The optimized framework of PHI-dual-2 exhibits a remarkable photocatalytic H_2O_2 production rate, which is 2.0 times of that on the active pristine PHI. The surface functionalization method is generally applicable to the modification of a wide range of polymeric carbon nitride frameworks with diverse compositions, and the best catalytic performance is observed on the thiourea derived K^+-doped polymeric carbon nitride with dual surface polarization sites; the H_2O_2 evolution rate could reach a remarkable high value of 40.5 mmol h^{-1} $g_{catal}{}^{-1}$. This work demonstrates a facile and efficient approach for boosting the photocatalytic performance of the carbon nitride frameworks, and also sheds light on the design of novel carbon nitride frameworks with outstanding photocatalytic activity *via* surface functionalization.

Declaration of competing interest

The authors declare that they have no financial and personal relationships with other people or organizations that can influence the work reported in this paper.

Acknowledgments

This work was financially supported by National Natural Science Foundation of China (No. 21976041), Guangzhou Municipal Science and Technology Project (No. 202201020168), Tertiary Education Scientific Research Project of Guangzhou Municipal Education Bureau (No. 202235238), and Guangdong Basic and Applied Basic Research Foundation (No. 2023A1515010788).

Supplementary materials

Supplementary material associated with this article can be found, in the online version, at doi:10.1016/j.cclet.2023.109251.

References

[1] C. Cao, X. Wang, N. Yang, et al., Chem. Sci. 13 (2022) 863–889.
[2] Y. Wen, F. Huo, C. Yin, Chin. Chem. Lett. 30 (2019) 1834–1842.
[3] Y. Xue, Y. Wang, Z. Pan, et al., Angew. Chem. Int. Ed. 60 (2021) 10469–10480.
[4] J.M. Campos-Martin, G. Blanco-Brieva, J.L. Fierro, Angew. Chem. Int. Ed. 45 (2006) 6962–6984.
[5] C. Xia, Y. Xia, P. Zhu, et al., Science 366 (2019) 226–231.
[6] X. Hu, X. Zeng, Y. Liu, et al., Nanoscale 12 (2020) 16008–16027.
[7] C. Huang, E. Fan, H. Xu, et al., Solid State Sci. 113 (2021) 106533.
[8] Y. Huang, Y. Jian, L. Li, et al., Angew. Chem. Int. Ed. 60 (2021) 5245–5249.
[9] H. Wang, Y. Xu, D. Xu, et al., ACS EST Eng. 2 (2022) 140–157.
[10] C. Zhao, Z. Chen, R. Shi, et al., Adv. Mater. 32 (2020) 1907296.
[11] S. Zhang, Y. Yang, Y. Zhai, et al., Chin. Chem. Lett. 34 (2023) 107652.
[12] X. Chen, W. Zhang, L. Zhang, et al., ACS Appl. Mater. Interfaces 13 (2021) 25868–25878.
[13] H. Cheng, H. Lv, J. Cheng, et al., Adv. Mater. 34 (2022) 2107480.
[14] K. Sahel, L. Elsellami, I. Mirali, et al., Appl. Catal. B 188 (2016) 106–112.
[15] J. Luo, C. Fan, L. Tang, et al., Appl. Catal. B 301 (2022) 120757.
[16] V. Briega-Martos, A. Ferre-Vilaplana, A. de la Peña, et al., ACS Catal. 7 (2017) 1015–1024.
[17] H. Zhang, L.H. Guo, L. Zhao, et al., J. Phys. Chem. Lett. 6 (2015) 958–963.
[18] Y. Kofuji, S. Ohkita, Y. Shiraishi, et al., ACS Sustain. Chem. Eng. 5 (2017) 6478–6485.
[19] L. Li, L. Xu, Z. Hu, et al., Adv. Funct. Mater. 31 (2021) 2106120.
[20] F. Liu, R. Shi, Z. Wang, et al., Angew. Chem. Int. Ed. 58 (2019) 11791–11795.
[21] Y. Shiraishi, T. Takii, T. Hagi, et al., Nat. Mater. 18 (2019) 985–993.
[22] Q. Tian, L. Jing, S. Ye, et al., Small 17 (2021) e2103224.
[23] L. Xu, Y. Liu, L. Li, et al., ACS Catal. 11 (2021) 14480–14488.
[24] C. Liu, T. Bao, L. Yuan, et al., Adv. Funct. Mater. 32 (2021) 2111404.
[25] L. Li, D. Cruz, A. Savateev, et al., Appl. Catal. B 229 (2018) 249–253.
[26] M. Li, Q. Zheng, D.P. Durkin, et al., J. Hazard. Mater. 436 (2022) 129251.
[27] X. Li, J. Zhang, Y. Huo, et al., Appl. Catal. B 280 (2021) 119452.
[28] Y. Fu, C.A. Liu, M. Zhang, et al., Adv. Energy Mater. 8 (2018) 1802525.
[29] D. Li, C. Wen, J. Huang, et al., Appl. Catal. B 307 (2022) 121099.
[30] K. Li, L. Bao, S. Cao, et al., ACS Appl. Energy Mater. 4 (2021) 12965–12973.
[31] L. Dai, A. Dong, X. Meng, et al., Angew. Chem. Int. Ed. 62 (2023) e202300224.
[32] J. Yang, A. Acharjya, M.Y. Ye, et al., Angew. Chem. Int. Ed. 60 (2021) 19797–19803.
[33] Q. Zhi, W. Liu, R. Jiang, et al., J. Am. Chem. Soc. 144 (2022) 21328–21336.
[34] Y. Zhao, P. Zhang, Z. Yang, et al., Nat. Commun. 12 (2021) 3701.
[35] Q. Wu, J. Cao, X. Wang, et al., Nat. Commun. 12 (2021) 483.
[36] Z. Teng, Q. Zhang, H. Yang, et al., Nat. Catal. 4 (2021) 374–384.
[37] F. Yu, L. Wang, Q. Xing, et al., Chin. Chem. Lett. 31 (2020) 1648–1653.
[38] G. Zhang, G. Li, T. Heil, et al., Angew. Chem. Int. Ed. 131 (2019) 3471–3475.
[39] A. Savateev, S. Pronkin, J.D. Epping, et al., ChemCatChem 9 (2017) 167–174.
[40] A. Savateev, S. Pronkin, M.G. Willinger, et al., Chem. Asian J. 12 (2017) 1517–1522.
[41] Z. Yang, L. Li, J. Cui, et al., Chem. Eur. J. 28 (2022) e202202122.
[42] Z. Yang, L. Li, J. Gao, et al., ACS EST Eng. 2 (2022) 2142–2149.
[43] Z. Yang, L. Li, S. Zeng, et al., ACS Appl. Mater. Interfaces 15 (2023) 8232–8240.
[44] C. Merschjann, S. Tschierlei, T. Tyborski, et al., Adv. Mater. 27 (2015) 7993–7999.
[45] R. Chen, Z. Ren, Y. Liang, et al., Nature 610 (2022) 296–301.
[46] S. Wu, H. Yu, S. Chen, et al., ACS Catal. 10 (2020) 14380–14389.
[47] J. Cheng, Y. Hou, K. Lian, et al., ACS Catal. 12 (2022) 1797–1808.
[48] K.C. Bedin, A.C. Martins, A.L. Cazetta, et al., Chem. Eng. J. 286 (2016) 476–484.
[49] L. Kong, J. Wang, Y. Jia, et al., J. Raman Spectrosc. 41 (2010) 989–995.
[50] Z. Zhai, H. Zhang, F. Niu, et al., ACS Nano 16 (2022) 21002–21012.
[51] L. Du, Q. Tian, X. Zheng, et al., Energy Environ. Mater. 5 (2021) 912–917.
[52] G. Zhang, Y. Xu, M. Rauf, et al., Adv. Sci. 9 (2022) e2201677.
[53] S. Gao, X. Wang, C. Song, et al., Appl. Catal. B 295 (2021) 120272.
[54] Z. Fang, Y. Bai, L. Li, et al., Nano Energy 75 (2020) 104865.
[55] W. Ren, J. Cheng, H. Ou, et al., J. Catal. 389 (2020) 636–645.
[56] L.L. Liu, F. Chen, J.H. Wu, et al., P. Natl. Acad. Sci. U. S. A. 120 (2023) e2215305120.
[57] X. He, H. Shang, C. Wang, et al., Chin. Chem. Lett. 32 (2021) 3377–3381.
[58] R.R. Pawar, Lalhmunsiama, M. Kim, et al., Appl. Clay Sci. 162 (2018) 339–350.
[59] S. Yu, J. Li, Y. Zhang, et al., Nano Energy 50 (2018) 383–392.
[60] J. Moan, E. Wold, Nature 279 (1979) 450–451.
[61] S. Trasatti, Pure Appl. Chem. 58 (1986) 955–966.
[62] H. Yu, R. Shi, Y. Zhao, et al., Adv. Mater. 29 (2017) 1605148.
[63] M.O. Eze, L.C. Nnamani, R.I. Ojiako, et al., Free Rad. Res. Cornms. 4 (1987) 105–108.
[64] R. Palominos, J. Freer, M.A. Mondaca, et al., J. Photoch. Photobio. A 193 (2008) 139–145.
[65] J. Luo, Y. Liu, C. Fan, et al., ACS Catal. 11 (2021) 11440–11450.